Radiation Oncology

RESEARCH

Open Access

Correlation between the γ passing rates of IMRT plans and the volumes of air cavities and bony structures in head and neck cancer

Zhengwen Shen, Xia Tan, Shi Li, Xiumei Tian, Huanli Luo, Ying Wang and Fu Jin*

Abstract

Background: Both patient-specific dose recalculation and γ passing rate analysis are important for the quality assurance (QA) of intensity modulated radiotherapy (IMRT) plans. The aim of this study was to analyse the correlation between the γ passing rates and the volumes of air cavities (V_{air}) and bony structures (V_{bone}) in target volume of head and neck cancer.

Methods: Twenty nasopharyngeal carcinoma and twenty nasal natural killer T-cell lymphoma patients were enrolled in this study. Nine-field sliding window IMRT plans were produced and the dose distributions were calculated by anisotropic analytical algorithm (AAA), Acuros XB algorithm (AXB) and SciMoCa based on the Monte Carlo (MC) technique. The dose distributions and γ passing rates of the targets, organs at risk, air cavities and bony structures were compared among the different algorithms.

Results: The γ values obtained with AAA and AXB were 95.6 ± 1.9% and 96.2 ± 1.7%, respectively, with 3%/2 mm criteria ($p > 0.05$). There were significant differences ($p < 0.05$) in the γ values between AAA and AXB in the air cavities (86.6 ± 9.4% vs. 98.0 ± 1.7%) and bony structures (82.7 ± 13.5% vs. 99.0 ± 1.7%). Using AAA, the γ values were proportional to the natural logarithm of V_{air} ($R^2 = 0.674$) and inversely proportional to the natural logarithm of V_{bone} ($R^2 = 0.816$). When the V_{air} in the targets was smaller than approximately 80 cc or the V_{bone} in the targets was larger than approximately 6 cc, the γ values of AAA were below 95%. Using AXB, no significant relationship was found between the γ values and V_{air} or V_{bone}.

Conclusion: In clinical head and neck IMRT QA, greater attention should be paid to the effect of V_{air} and V_{bone} in the targets on the γ passing rates when using different dose calculation algorithms.

Keywords: IMRT QA, γ passing rates, Air cavities, Bony structures, Monte Carlo

Introduction

Radiation dose escalation has been shown to be beneficial for local control and improving overall survival in the treatment of cancer [1, 2]. However, these benefits may be accompanied by higher incidences of acute and late toxicity [3, 4]. Intensity modulated radiation therapy (IMRT) results in desirable target coverage and toxicity reduction to organs at risk (OARs), but it is associated with many uncertainties leading to dose deviations that affect predictions about tumour control probability (TCP) and normal tissue complication probability (NTCP). The American Association of Physicists in Medicine (AAPM) Task Group 40 report (TG-40) recommends that the dose delivered to patients should be within 5% of the prescribed dose [5], but such an accurate and consistent dose delivery is complicated, since many steps are involved during the treatment process; therefore, the dose deviations produced at each step should be

*Correspondence: jfazj@cqu.edu.cn
Department of Radiation Oncology, Chongqing University Cancer Hospital, Chongqing 400030, China

as small as possible. Continually updated guidelines have been provided to assure the accuracy of radiation treatment [6–12]; most focus on device evaluations and dose measurements, but few address the accuracy of the dose calculation algorithms. The human body is composed of different components, which increases the challenge of accurate calculation. Hence, in the quality assurance (QA) of the treatment planning system (TPS), the evaluation of the accuracy of the dose distribution produced by the TPS is indispensable.

Nasopharyngeal carcinoma (NPC) and nasal natural killer T-cell lymphoma (NNKTCL) are both characterized by regional and ethnic differences; the two cancers are more common in Eastern Asia than in Western countries, demonstrating a particularly high incidence in southern China [13, 14]. NPC and NNKTCL represent the major head and neck cancers commonly treated by IMRT. Respiratory and organ movement have little impact on setup errors for IMRT in head and neck cancer. Given the good performance of the equipment and correct operation by the therapists, dose deviations are thus mainly caused by the dose calculation algorithms. The target region for NPC and NNKTCL includes a considerable number of air cavities and bony structures, resulting in three heterogeneous interfaces: air–tissue, bone–tissue and air-bone. Radiation beams passing through these heterogeneous interfaces always lead to the electronic disequilibrium effect and dose perturbations.

To our knowledge, patient-specific dose recalculation using the Monte Carlo (MC) algorithm, as a step of IMRT QA, for head and neck cancer has not been investigated [15–17]. Therefore, one of our aims was to implement this QA step in real patients with NPC and NNKTCL using the MC method. Numerous studies have investigated the assessment of dose perturbations at heterogeneous interfaces [18–20]; however, studies that compared the results produced by TPS against measured data in heterogeneous media have typically focused on the agreement in the area around the heterogeneity, and only a few have investigated the agreement directly within the heterogeneity. Therefore, another aim of our study was to compare the dosimetric difference directly inside air cavities and bony structures based on the QA results and analyse the correlation between the γ passing rates and the volume of the air cavities (V_{air}) and bony structures (V_{bone}).

Materials and methods

Patients and prescription

Twenty NPC patients and twenty NNKTCL patients were selected from the clinical database. All patients underwent CT scans with a 3 mm slice thickness. Three planning target volumes were defined for each NPC patient with 70.4 Gy prescribed to PGTVnx and PGTVnd, 60.8 Gy to PTV1, and 54.4 Gy to PTV2 in 32 daily fractions. For each NNKTCL patient, the prescribed PTV dose was 56 Gy in 28 daily fractions.

The volumes of the contoured PGTVnx for NPC and the PTV for NNKTCL included a considerable number of air cavities and bony structures. To assess the dosimetric impact on these volumes, the air cavities and bony structures included in PGTVnx and PTV were contoured separately. Since PGTVnx contained the largest proportion of air cavities and bony structures relative to the other targets with lower dose prescriptions among the NPC patients, the analysis was confined to PGTVnx in this study.

Treatment planning

All plans were generated using 6 MV photon beams and modulated with a Millennium 120 multi-leaf collimator (MLC) from a Varian Clinac IX (Varian Medical Systems, Palo Alto, California, USA) in Eclipse TPS version 15.6. The plans were created using nine fields that were evenly distributed in coplanar directions with the sliding window technique. Because the lenses and optic nerves were close to the PTV for NNKTCL patients, the angle of the collimator and the position of the jaws in some fields were adjusted, and fixed jaws were used during optimization.

The optimization goal was to ensure that at least 95% of the volume of the targets received the prescribed dose and that the maximal dose of the targets would not exceed 110% of the prescribed dose, while minimizing the doses to the OARs, whose dose constraints are given in Table 1. After optimization, dose calculations were performed using anisotropic analytical algorithm (AAA) version 15.6.06 with a 2.5 mm grid size. The quality of each plan was assessed with regard to its clinical acceptability by oncologists. Each plan was subsequently recalculated using Acuros XB algorithm (AXB) version 15.6.06 (dose to medium), using the same calculation settings as AAA.

Table 1 Dose constraints for the organs at risk

OARs	Constraints	OARs	Constraints
Brainstem	D_{max}<54Gy	Spinal cord	D_{max}<40Gy
Optic chiasm	D_{max}<54Gy	Optic nerves	D_{max}<54Gy
Pituitary	D_{max}<54Gy	Eyes	D_{mean}<25Gy
Temporal lobes	V_{60}<2cc	Parotid glands	D_{mean}<30Gy
Lens	D_{max}<12Gy	Inner ears	D_{mean}<35Gy
Oral cavity	D_{mean}<38Gy	Mandible	V_{55}<10%

SciMoCa model and dose recalculation

The SciMoCa algorithm for linear accelerators is described in detail in Ref. [21, 22]. It combines the concepts of the voxel-based Monte Carlo algorithm with some element of EGSnrc [23]. The treatment head simulation, employing five virtual sources determined from BEAMnrc, is an evolution from previous models [24, 25]. The 6 MV beam modality of the Varian Clinac IX with the Millennium 120 MLC was commissioned using the same measurement data used to commission the Eclipse TPS. The accelerator head was commissioned on the basis of depth dose curves, profile curves measured at five depths (1.5, 5, 10, 20, 30 cm) and output factors for square fields (3×3, 5×5, 10×10, 15×15, 20×20, 30×30, 40×40 mm^2). The dosimetry leaf gap and leaf transmission of the MLC were configured to match the measured data [26].

The selected plans were exported to SciMoCa and recalculated using the DICOM images, structure sets and plan information. The dose was reported as dose to medium. The grid size of 2.5 mm used for the calculation was the same as that of TPS. SciMoCa can employ uncertainty levels of 2%, 1%, and 0.5%. Smaller the statistical uncertainty is, the more accurate the MC calculation. To obtain the most accurate QA results, the 0.5% statistical uncertainty level was used in our study.

Dosimetric evaluation and data analysis

For the forty real patient plans (twenty NPC and twenty NNKTCL plans), the dosimetric parameters mentioned in Table 1 were compared. The results of the calculation from MC were used as the reference data sets, and the results of the calculation from AAA and AXB were used as the evaluated data sets. The dose distributions from AAA and AXB were compared with those of MC using a global γ evaluation with suppression of doses below 10% of the maximum dose. The percentage of points fulfilling the γ evaluation was scored as the γ passing rate. It has been recommended that the γ passing rates should be $\geq$ 95% with a dose difference of 3% and a distance to agreement of 2 mm (3%/2 mm) [12]. The γ passing rates were scored for the entire plan and for the targets and OARs. The mean dose to the air cavities and bony structures in the targets estimated by AAA and AXB were calculated and compared with that estimated by MC for each patient. The γ passing rates were also scored separately for the air cavities and bony structures. Scatter plots were used to explore the correlation between the γ passing rates and V_{air}/V_{bone}.

The paired *t*-test was used to determine if there was a significant difference for each of the parameters. $p<0.05$ was considered statistically significant. SPSS statistical software (SPSS, Chicago, IL, USA) was used for all analyses.

Results

γ evaluation results

Table 2 summarizes the γ passing rates for forty clinical head and neck cancer patients using AAA and AXB for the entire plan and for the targets sand OARs. The γ passing rates from AXB were higher than those from AAA. The γ values from AAA for the entire plan and for the targets and OARs were over 95%, except for PGTVnx and PTV. Table 2 also shows that the γ evaluation results from AAA and AXB for PGTVnx, PTV1, PTV, mandible and oral cavity were statistically significant.

Dosimetric comparison

Table 3 summarizes the dose parameters of the targets and OARs and the number of plans satisfying the clinical requirements. The dose estimated by AXB provided better agreement with MC than AAA. AXB estimated a 0.1%~1.5% lower target coverage and a 1.6~3.5 Gy higher target D_{max} than AAA. The D_{max} estimated by AXB to the serial organs, including the brain stem, spinal cord, optic chiasm, optic nerves, lens and pituitary was

Table 2 γ passing rates for entire plans, targets and OARs. (%)

	AAA	AXB	*p* value
Entire plans	95.6±1.9	96.2±1.7	>0.05
PGTVnx	93.8±2.3	99.6±0.2	<0.05
PGTVnd	98.9±1.1	99.3±0.7	>0.05
PTV1	97.3±1.3	99.7±0.2	<0.05
PTV2	98.2±0.8	98.9±0.9	>0.05
PTV	90.3±6.2	97.2±5.3	<0.05
Brain stem	99.9±0.3	99.9±0.2	>0.05
Spinal cord	96.9±2.9	97.0±3.2	>0.05
Optic chiasm	99.9±0.2	99.9±0.2	>0.05
Left optic nerve	100±0	100±0	>0.05
Right optic nerve	99.9±0.4	100±0	>0.05
Pituitary	99.7±0.3	100±0	>0.05
Left len	99.5±0.3	99.7±0.2	>0.05
Right len	99.6±0.2	99.9±0.2	>0.05
Left eye	99.3±2.6	99.3±2.3	>0.05
Right eye	99.3±2.1	99.3±2.1	>0.05
Left temporal lobe	99.8±0.1	99.9±0.1	>0.05
Right temporal lobe	99.8±0.4	99.9±0.2	>0.05
Mandible	98.3±0.7	99.8±0.4	<0.05
Left parotid gland	99.0±1.5	99.6±0.6	>0.05
Right parotid gland	99.4±0.9	99.7±0.4	>0.05
Left inner ear	99.7±0.6	100±0	>0.05
Right inner ear	99.7±0.6	100±0	>0.05
Oral cavity	96.7±0.8	99.2±0.5	<0.05

Table 3 Summary of the doses to the targets and OARs estimated by AAA, AXB and MC

Structure	Parameter	AAA	AXB	MC
PGTVnx	$V_{70.4}$, %	97.9±2.3 (19)	96.7±2.9 (17)	96.7±3.0 (16)
	D_{max}, Gy	75.8±1.4 (20)	77.4±1.4 (15)	77.4±1.5 (13)
PGTVnd	$V_{70.4}$, %	97.3±1.1 (20)	96.7±2.4 (17)	96.6±2.8 (17)
	D_{max}, Gy	75.6±1.5 (20)	77.2±1.3 (20)	77.6±1.2 (15)
PTV1	$V_{60.8}$, %	95.9±1.5 (18)	95.8±1.3 (17)	95.6±1.5 (17)
PTV2	$V_{54.4}$, %	95.5±2.3 (15)	94.7±2.2 (13)	94.1±2.4 (11)
PTV	V_{56}, %	94.6±2.6 (17)	92.1±4.5 (16)	90.9±6.9 (15)
	D_{max}, Gy	61.3±2.5 (15)	64.8±4.1 (13)	65.5±5.5 (12)
Brain stem	D_{max}, Gy	46.9±13.8 (36)	47.2±13.8 (35)	47.5±14.1 (35)
Spinal cord	D_{max}, Gy	32.7±11.4 (39)	32.8±11.4 (39)	33.2±11.3 (38)
Optic chiasm	D_{max}, Gy	48.4±13.3 (40)	48.5±13.1 (40)	49.0±13.3 (39)
Left optic nerve	D_{max}, Gy	43.2±16.0 (38)	43.4±16.1 (36)	43.4±16.2 (36)
Right optic nerve	D_{max}, Gy	41.0±16.0 (38)	41.2±16.2 (38)	41.5±16.2 (38)
Pituitary	D_{max}, Gy	54.8±9.8 (27)	55.4±9.6 (26)	56±9.9 (26)
Left len	D_{max}, Gy	9.0±2.7 (37)	9.7±3.0 (36)	9.8±2.5 (35)
Right len	D_{max}, Gy	11.2±10.5 (35)	11.5±10.5 (33)	11.8±11.1 (33)
Left eye	D_{mean}, Gy	12.8±4.2 (40)	12.6±4.2 (40)	12.4±4.3 (40)
Right eye	D_{mean}, Gy	13.6±5.6 (40)	13.4±5.6 (40)	13.2±5.7 (40)
Left temporal lobe	V_{60}, cc	0.3±0.7 (37)	0.3±0.8 (37)	0.3±0.8 (37)
Right temporal lobe	V_{60}, cc	0.2±0.6 (38)	0.2±0.6 (38)	0.2±0.5 (38)
Mandible	V_{55}, %	2.4±4.2 (39)	2.4±4.4 (39)	2.4±4.1 (39)
Left parotid gland	D_{mean}, Gy	16.0±16.5 (29)	15.9±16.6 (29)	15.8±16.6 (29)
Right parotid gland	D_{mean}, Gy	16.2±16.5 (27)	16.0±16.6 (27)	15.8±16.5 (27)
Left inner ear	D_{mean}, Gy	22.7±15.7 (25)	22.5±15.7 (26)	22.5±15.7 (26)
Right inner ear	D_{mean}, Gy	22.2±14.6 (25)	21.8±14.6 (26)	21.5±14.5 (26)
Oral cavity	D_{mean}, Gy	32.0±14.0 (40)	31.6±13.8 (40)	31.3±13.6 (40)

The numbers in brackets counted the plans satisfying the clinical requirements

0.1 ~ 0.7 Gy higher than that estimated by AAA. Using AXB, the estimated mean doses to the eyes, parotid glands, inner ears and oral cavity were 0.1 ~ 0.4 Gy lower than those estimated by AAA. V_{60} for the temporal lobes and V_{55} for the mandible provided by the three different methods were the same. The number of plans satisfying the clinical requirements calculated by AXB was no more than that calculated by AAA.

Table 4 summarizes the D_{mean} differences and γ passing rates of the air cavities and bony structures in the targets for all forty patients. The D_{mean} to the air cavities was underestimated by 1.6% using AAA and by 0.2% using AXB, and the D_{mean} to the bony structures was overestimated by 2.3% using AAA and by 0.4% using AXB with respect to the benchmark MC values. The γ passing rates of AXB were higher than those of AAA, indicating that the doses to the air cavities and bony structures in the targets calculated by AXB were more accurate than those calculated by AAA.

Table 4 D_{mean}differences and γ passing rates of the air cavities and bony structures

	V (cc)	Diff (%)			γ (%)		
		AAA	AXB	*p* value	AAA	AXB	*p* value
Air cavities	36.7±36.1	-1.6±0.5	-0.2±0.6	<0.05	86.6±9.4	98.0±1.7	<0.05
Bony structures	41.2±37.9	2.3±0.7	0.4±0.4	<0.05	82.7±13.5	99.0±1.7	<0.05

Diff = (D_{mean}(TPS) –D_{mean}(MC))/ D_{mean} (MC) ×100%

Correlation analysis

Figures 1 and 2 show scatter plots with fitted curves for the γ passing rates using AAA and AXB versus V_{air} and V_{bone}. The V_{air} and V_{bone} of NPC were smaller than those of NNKTCL. It can be seen from Figs. 1a and 2a that, using AAA, the γ passing rates were proportional to the natural logarithm of V_{air} ($R^2 = 0.674$) and inversely proportional to the natural logarithm of V_{bone} ($R^2 = 0.816$). For the 20 NPC patients and 20 NNKTCL patients assessed using AAA separately, the R^2 values were 0.314 and 0.434 for the air cavities and 0.711 and 0.655 for the bony structures, respectively, which were less than the R^2 values when the volume were regarded as a whole. The small R^2 values of AXB are showed in Figs. 1b and 2b, indicating a negligible correlation between the γ passing rates and V_{air}/V_{bone}.

Discussion

Several studies have reported that 5% changes in the dose calculation may result in 20% changes in the local tumour control probability and 30% changes in the normal tissue complication probability [15, 16]. Accurate dose calculations are fundamental for radiotherapy treatment planning and it has been suggested that the error of dose calculation be less than 3% [27]. Thus, it is essential to implement patient-specific dose recalculation QA to ensure acceptable calculation results by the TPS. The MC method was used for our dose recalculation QA and taken as the benchmark to investigate the dose distributions of head and neck IMRT plans produced by AAA and AXB. Finally, the correlation between the γ passing rates and V_{air}/V_{bone} in targets was explored based on our QA results.

Following the reporting and integration of AXB into the Eclipse TPS [28], studied have investigated and

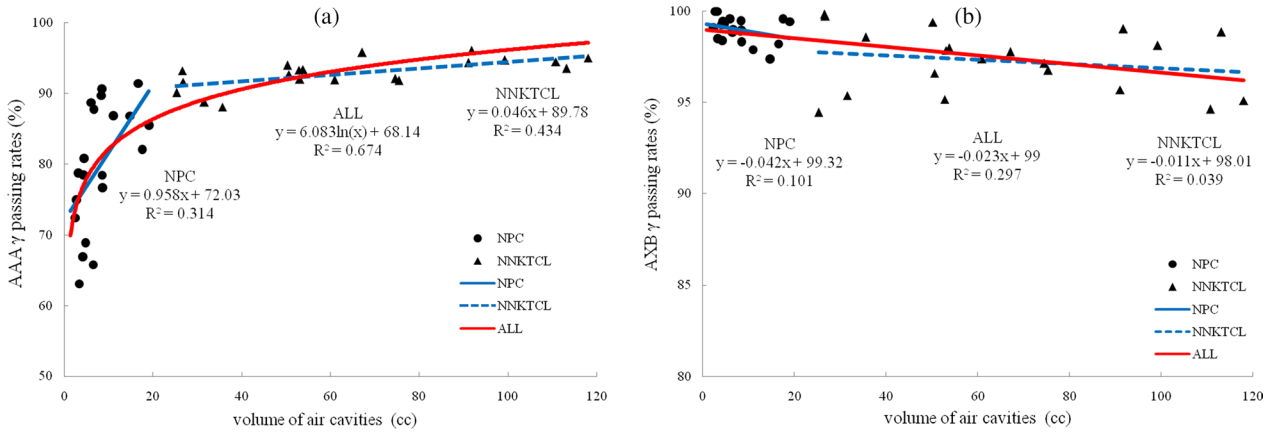

Fig. 1 Scatter plots with fitted curves for γ passing rates and V_{air} using AAA (**a**) and AXB (**b**)

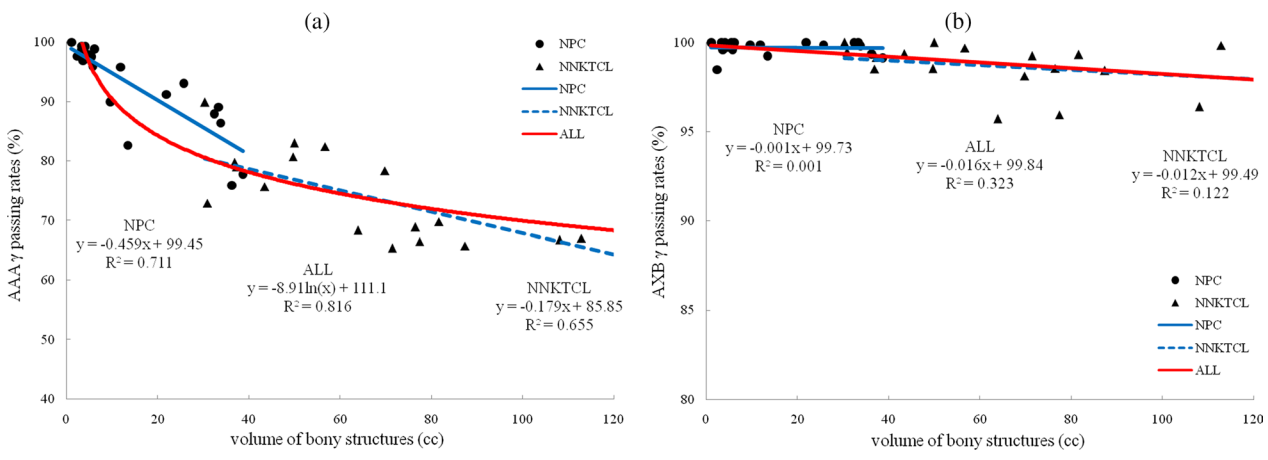

Fig. 2 Scatter plots with fitted curves for γ passing rates and V_{bone} using AAA (**a**) and AXB (**b**)

compared the calculation results provided by AAA and AXB. For a single field in heterogeneous media, AXB performed better than AAA due to better optimizations for the lateral electronic disequilibrium effect [29–31]. However, the effect was compensated when clinical IMRT plans are created with multiple fields from different directions, so the difference between AAA and AXB may not be obvious. Other experiments demonstrated that both algorithms produced acceptable accuracy with respect to the measured data [32–35]. However, dosimetric measurements introduced several challenges, such as the position of measurement and the particle disequilibrium caused by the inserted material [36].

Some investigations have revealed the dosimetric differences between AAA and AXB in real patients with head and neck cancers [19, 34, 35], but these differences need to be benchmarked against the gold standard, the MC method. AXB algorithm and Monte Carlo method can both report the absorbed dose in two modes: dose to medium and dose to water. Han et al. [33] reported verification results for AXB using the Radiological Physics Center head and neck phantom. The dose distributions predicted by AXB with both dose to medium and dose to water modes were compared to the doses measured using thermo luminescent dosimeters and films. The authors observed that the dose to medium mode produced slightly better agreement with the measurement results than the dose to water mode. Ma et al. [37] suggested that to achieve consistency with previous radiation therapy experiences, MC photon algorithms should report using dose to medium mode for treatment plan evaluation and treatment outcome analysis. Therefore, AXB and MC algorithms were configured to report in the dose to medium mode in our research.

Our patient-specific dose recalculation QA results showed that the target coverage produced by AXB had better agreement with MC than AAA. However, the prescribed dose coverage of PGTVnx and PTV produced by AXB were 1.2% and 2.5% lower, respectively, than that produced by AAA, which was expected according to the results of previous studies [19, 34, 35]. The γ passing rates of AAA and AXB for PGTVnx and PTV were statistically significant because these regions presented with many air cavities and bony structures, affecting accurate dose calculations. PTV1 contained PGTVnx, so the γ evaluation of AAA and AXB for PTV1 also showed statistical significance.

It should be noted that in this study, the D_{max} values of the targets and serial OARs (brain stem, spinal cord, optic chiasm, optic nerves, pituitary and lens) predicted by AXB were all greater than those predicted by AAA, which was not consistent with previous literature [19, 34, 35]. A D_{max} of the target exceeding 110% of the prescribed dose would be moderately acceptable; however, the calculation of different D_{max} values for serial OARs by different algorithms requires dose recalculation QA checks to ensure patient safety. It is more acceptable and reasonable to assess clinical plans with $V_{110\%}$ for high dose regions of targets and $D_{1\%}$ for serial OARs. In contrast, the D_{mean} of parallel OARs (eyes, parotid glands, inner ears and oral cavity) predicted by AXB was smaller than that predicted by AAA, and the V_{60} of the temporal lobes and V_{55} of the mandible predicted by AXB were equal to those predicted by AAA. Using AAA and AXB, the γ values of the mandible and oral cavity were all > 95%, which attracting less attention than the targets and priority 1 OARs [38]. However, the statistical significance of the γ values for the mandible and oral cavity calculated by both AAA and AXB also reflected the different performances of AAA and AXB in the air cavities and bony structures.

Previous investigations have observed better agreement between AXB and MC within extremely low or high density materials [29–31]. Our study demonstrated that the air cavities and bony structures had an impact on the accurate dose calculation by AAA for both the targets and OARs in clinical IMRT plans. Although the dosimetric parameters produced by AAA tended to satisfy clinical requirements, those produced by AXB and MC were more consistent.

Compared with the MC algorithm, AAA and AXB underestimated the D_{mean} inside the air cavities by 1.6% and 0.2% and overestimated the D_{mean} inside the bony structures by 2.3% and 0.4%, respectively. Figures 1 and 2 show the relationship between the γ passing rates and V_{air}/V_{bone} more clearly. From the scatter plots for AAA, whether separately or jointly for NPC and NNKTCL, the larger V_{air} was or the smaller V_{bone} was, the higher the γ passing rate was. However, a negligible correlation was found between the γ values predicted by AXB and V_{air}/V_{bone}, indicating that the air cavities and bony structures had little impact on the accurate dose calculation of AXB. The γ passing rates from AAA were proportional to the natural logarithm of V_{air} and inversely proportional to the natural logarithm of V_{bone}. When V_{air} in the targets was smaller than approximately 80 cc or V_{bone} was larger than approximately 6 cc, the γ values from AAA were below 95%.

The V_{air} and V_{bone} of NPC were generally smaller than those of NNKTCL because of differences in the target location. Therefore, the curves of the γ values versus V_{air}/V_{bone} for NPC and NNKTCL were fitted separately. NPC and NNKTCL are both head and neck cancers, however, and when they were considered as a whole, higher R^2 values were obtained for the fitted curves. This suggested that the relationship between the γ values and V_{air}/V_{bone} discovered in this study may

be present in other head and neck cancers, but this remains to be further explored.

In addition, we compared 0.5% uncertainty with 2% uncertainty of the MC method to clarify the impact of statistical uncertainty on the relationship between the γ values and V_{air} or V_{bone}. Using 2% statistical uncertainty, the γ values from AAA in the air cavities and bony structures were decreased by $5.7 \pm 4.3\%$ and $5.3 \pm 4.1\%$, respectively, and the corresponding γ values from AXB were decreased by $4.5 \pm 3.1\%$ and $3.7 \pm 2.8\%$. The dose discrepancies caused by statistical uncertainty were obvious; therefore it is necessary to set the statistical uncertainty of the MC method as small as possible. The accuracy of dose calculation should be traded off for time. However, using 2% statistical uncertainty, the γ values from AAA were still proportional to the natural logarithm of V_{air} and inversely proportional to the natural logarithm of V_{bone} but with slightly lower R^2 values, and there remained a negligible correlation between the γ values from AXB and V_{air}/V_{bone}.

Conclusion

To ensure that the deviation between the actual dose given to the patient and the dose distribution calculated by the TPS is within reasonable limits, patient-specific dose recalculation QA must be implemented. The dose discrepancies caused by the air cavities and bony structures need to be considered when using different dose algorithms. In clinical QA practice, the effect of V_{air} and V_{bone} in the targets on γ passing rates should be considered.

Acknowledgements
Not applicable.

Authors' contributions
All authors contributed to the study. Zhengwen Shen drafted the manuscript. Fu Jin revised the manuscript. All authors read and approved the final manuscript.

Funding
This work is supported by the National Natural Science Foundation of China under grant No. 11805025 and 81972857.

Availability of data and material
The datasets used during this study are available from the corresponding author on reasonable request.

Ethics approval and consent to participate
Not applicable.

Consent for publication
Not applicable.

Competing interests
The authors declare that they have no competing interests.

Received: 14 May 2021 Accepted: 15 July 2021
Published online: 21 July 2021

References

1. Jin F, Luo H, Zhou J, et al. Dose-time fractionation schedules of preoperative radiotherapy and timing to surgery for rectal cancer. Ther Adv Med Oncol. 2020;12:1758835920907537.
2. Bourhis J, Overgaard J, Audry H, et al. Hyperfractionated or accelerated radiotherapy in head and neck cancer: a meta-analysis. Lancet. 2006;368(9538):843–54.
3. Chen NB, Qiu B, Zhang J, et al. Intensity-Modulated Radiotherapy versus Three-Dimensional Conformal Radiotherapy in Definitive Chemoradiotherapy for Cervical Esophageal Squamous Cell Carcinoma: Comparison of Survival Outcomes and Toxicities. Cancer Res Treat. 2020;52(1):31–40.
4. Pasalic D, Betancourt-Cuellar SL, Taku N, et al. Outcomes and toxicities following stereotactic ablative radiotherapy for pulmonary metastases in patients with primary head and neck cancer. Head Neck. 2020;42(8):1939–53.
5. Kutcher GJ, Coia L, Gillin M, et al. Comprehensive QA for radiation oncology: report of AAPM Radiation Therapy Committee Task Group 40. Med Phys. 1994;21(4):581–618.
6. Nath R, Biggs PJ, Bova FJ, et al. AAPM code of practice for radiotherapy accelerators: report of AAPM Radiation Therapy Task Group No. 45. Med Phys. 1994;21(7):1093–1121.
7. Almond PR, Biggs PJ, Coursey BM, et al. AAPM's TG-51 protocol for clinical reference dosimetry of high-energy photon and electron beams. Med Phys. 1999;26(9):1847–70.
8. Fraass B, Doppke K, Hunt M, et al. American Association of Physicists in Medicine Radiation Therapy Committee Task Group 53: quality assurance for clinical radiotherapy treatment planning. Med Phys. 1998;25(10):1773–829.
9. Benedict SH, Yenice KM, Followill D, et al. Stereotactic body radiation therapy: the report of AAPM Task Group 101. Med Phys. 2010;37(8):4078–101.
10. Low DA, Moran JM, Dempsey JF, Dong L, Oldham M. Dosimetry tools and techniques for IMRT. Med Phys. 2011;38(3):1313–38.
11. Klein EE, Hanley J, Bayouth J, et al. Task Group 142 report: quality assurance of medical accelerators. Med Phys. 2009;36(9):4197–212.
12. Miften M, Olch A, Mihailidis D, et al. Tolerance limits and methodologies for IMRT measurement-based verification QA: Recommendations of AAPM Task Group No. 218. Med Phys. 2018;45(4):e53-e83.
13. Yao JJ, Qi ZY, Liu ZG, et al. Clinical features and survival outcomes between ascending and descending types of nasopharyngeal carcinoma in the intensity-modulated radiotherapy era: A big-data intelligence platform-based analysis. Radiother Oncol. 2019;137:137–44.
14. Liu X, Huang E, Wang Y, et al. Dosimetric comparison of helical tomotherapy, VMAT, fixed-field IMRT and 3D-conformal radiotherapy for stage I-II nasal natural killer T-cell lymphoma. Radiat Oncol. 2017;12(1):76.
15. Haga A, Magome T, Takenaka S, et al. Independent absorbed-dose calculation using the Monte Carlo algorithm in volumetric modulated arc therapy. Radiat Oncol. 2014;9:75.
16. Kry SF, Glenn MC, Peterson CB, et al. Independent recalculation outperforms traditional measurement-based IMRT QA methods in detecting unacceptable plans. Med Phys. 2019;46(8):3700–8.
17. Kry SF, Molineu A, Kerns JR, et al. Institutional patient-specific IMRT QA does not predict unacceptable plan delivery. Int J Radiat Oncol Biol Phys. 2014;90(5):1195–201.
18. Yan C, Combine AG, Bednarz G, et al. Clinical implementation and evaluation of the Acuros dose calculation algorithm. J Appl Clin Med Phys. 2017;18(5):195–209.
19. Kan MW, Leung LH, Yu PK. Dosimetric impact of using the Acuros XB algorithm for intensity modulated radiation therapy and RapidArc planning in nasopharyngeal carcinomas. Int J Radiat Oncol Biol Phys. 2013;85(1):e73–80.
20. Tsuruta Y, Nakata M, Nakamura M, et al. Dosimetric comparison of Acuros XB, AAA, and XVMC in stereotactic body radiotherapy for lung cancer. Med Phys. 2014;41(8):081715.
21. Hoffmann L, Alber M, Söhn M, Elstrøm UV. Validation of the Acuros XB dose calculation algorithm versus Monte Carlo for clinical treatment plans. Med Phys. 2018;45(8):3909–15.
22. Sikora M, Dohm O, Alber M. A virtual photon source model of an Elekta linear accelerator with integrated mini MLC for Monte Carlo based IMRT dose calculation. Phys Med Biol. 2007;52(15):4449–63.

23. Kawrakow I, Fippel M. Investigation of variance reduction techniques for Monte Carlo photon dose calculation using XVMC. Phys Med Biol. 2000;45(8):2163–83.
24. Kawrakow I. Improved modeling of multiple scattering in the Voxel Monte Carlo model. Med Phys. 1997;24(4):505–17.
25. Sikora M, Alber M. A virtual source model of electron contamination of a therapeutic photon beam. Phys Med Biol. 2009;54(24):7329–44.
26. Piffer S, Casati M, Marrazzo L, et al. Validation of a secondary dose check tool against Monte Carlo and analytical clinical dose calculation algorithms in VMAT. J Appl Clin Med Phys. 2021;22(4):52–62.
27. Chetty IJ, Curran B, Cygler JE, et al. Report of the AAPM Task Group No. 105: Issues associated with clinical implementation of Monte Carlo-based photon and electron external beam treatment planning. Med Phys. 2007;34(12):4818–4853.
28. Vassiliev ON, Wareing TA, McGhee J, Failla G, Salehpour MR, Mourtada F. Validation of a new grid-based Boltzmann equation solver for dose calculation in radiotherapy with photon beams. Phys Med Biol. 2010;55(3):581–98.
29. Fogliata A, Nicolini G, Clivio A, Vanetti E, Cozzi L. Dosimetric evaluation of Acuros XB Advanced Dose Calculation algorithm in heterogeneous media. Radiat Oncol. 2011;6:82.
30. Bush K, Gagne IM, Zavgorodni S, Ansbacher W, Beckham W. Dosimetric validation of Acuros XB with Monte Carlo methods for photon dose calculations. Med Phys. 2011;38(4):2208–21.
31. Han T, Mikell JK, Salehpour M, Mourtada F. Dosimetric comparison of Acuros XB deterministic radiation transport method with Monte Carlo and model-based convolution methods in heterogeneous media. Med Phys. 2011;38(5):2651–64.
32. Alhakeem EA, AlShaikh S, Rosenfeld AB, Zavgorodni SF. Comparative evaluation of modern dosimetry techniques near low- and high-density heterogeneities. J Appl Clin Med Phys. 2015;16(5):142–58.
33. Han T, Mourtada F, Kisling K, Mikell J, Followill D, Howell R. Experimental validation of deterministic Acuros XB algorithm for IMRT and VMAT dose calculations with the Radiological Physics Center's head and neck phantom. Med Phys. 2012;39(4):2193–202.
34. Kan MW, Leung LH, So RW, Yu PK. Experimental verification of the Acuros XB and AAA dose calculation adjacent to heterogeneous media for IMRT and RapidArc of nasopharygeal carcinoma. Med Phys. 2013;40(3):031714.
35. Kan MW, Leung LH, Yu PK. Verification and dosimetric impact of Acuros XB algorithm on intensity modulated stereotactic radiotherapy for locally persistent nasopharyngeal carcinoma. Med Phys. 2012;39(8):4705–14.
36. Delbaere A, Younes T, Vieillevigne L. On the conversion from dose-to-medium to dose-to-water in heterogeneous phantoms with Acuros XB and Monte Carlo calculations. Phys Med Biol. 2019;64(19):195016.
37. Ma CM, Li J. Dose specification for radiation therapy: dose to water or dose to medium? Phys Med Biol. 2011;56(10):3073–89.
38. Lee AW, Ng WT, Pan JJ, et al. International Guideline on Dose Prioritization and Acceptance Criteria in Radiation Therapy Planning for Nasopharyngeal Carcinoma. Int J Radiat Oncol Biol Phys. 2019;105(3):567–80.

Publisher's Note